Remote nongenetic optical modulation of neuronal activity using fuzzy graphene

Sahil K. Rastogi[a,1], Raghav Garg[b,1], Matteo Giuseppe Scopelliti[c], Bernardo I. Pinto[d], Jane E. Hartung[e], Seokhyoung Kim[f], Corban G. E. Murphey[f], Nicholas Johnson[b], Daniel San Roman[b], Francisco Bezanilla[d], James F. Cahoon[f], Michael S. Gold[e], Maysam Chamanzar[c], and Tzahi Cohen-Karni[a,b,2]

[a]Department of Biomedical Engineering, Carnegie Mellon University, Pittsburgh, PA 15213; [b]Department of Materials Science and Engineering, Carnegie Mellon University, Pittsburgh, PA 15213; [c]Department of Electrical and Computer Engineering, Carnegie Mellon University, Pittsburgh, PA 15213; [d]Department of Biochemistry and Molecular Biology, University of Chicago, Chicago, IL 60637; [e]Department of Neurobiology, University of Pittsburgh, Pittsburgh, PA 15213; and [f]Department of Chemistry, University of North Carolina at Chapel Hill, Chapel Hill, NC 27599-3290

Edited by John A. Rogers, Northwestern University, Evanston, IL, and approved April 28, 2020 (received for review March 23, 2020)

The ability to modulate cellular electrophysiology is fundamental to the investigation of development, function, and disease. Currently, there is a need for remote, nongenetic, light-induced control of cellular activity in two-dimensional (2D) and three-dimensional (3D) platforms. Here, we report a breakthrough hybrid nanomaterial for remote, nongenetic, photothermal stimulation of 2D and 3D neural cellular systems. We combine one-dimensional (1D) nanowires (NWs) and 2D graphene flakes grown out-of-plane for highly controlled photothermal stimulation at subcellular precision without the need for genetic modification, with laser energies lower than a hundred nanojoules, one to two orders of magnitude lower than Au-, C-, and Si-based nanomaterials. Photothermal stimulation using NW-templated 3D fuzzy graphene (NT-3DFG) is flexible due to its broadband absorption and does not generate cellular stress. Therefore, it serves as a powerful toolset for studies of cell signaling within and between tissues and can enable therapeutic interventions.

graphene | nanowire | optical modulation | dorsal root ganglia neurons | spheroids

Cell–cell communication is fundamental to the emergence of higher-order function in tissue. Since Hodgkin and Huxley's (1) seminal work on the electrical activity of squid giant axons, input/output interfaces with electroactive cells and tissues have steadily improved through a variety of techniques and materials, enabling increased spatial and temporal control (2). The development of optogenetics (3) has revolutionized our ability to control the activity in excitable cells and tissues and fundamentally changed the questions that we can ask and answer. Clinical translation potential of optogenetics is limited, since it requires genetic modification of the cells or organisms to introduce the light-sensitive proteins (3, 4). Similarly, magnetogenetics, which uses superparamagnetic nanoparticles for localized heating and stimulation (5, 6), has enhanced our ability to modulate cellular activity, but it also requires genetic modification, that is, expression of the heat-sensitive transient receptor potential ion channel (TRPV1). It also is limited by a relatively long latency of up to 5 s between the magnetic field application and the onset of neural activity (5). As an alternative to genetic modification, direct infrared (IR) laser pulses are used to induce membrane depolarization (7, 8). However, direct IR stimulation does not provide cell specificity, spatial stimulation precision, or subcellular resolution, and suffers from a narrow energy density threshold for stimulation vs. damage to the tissue (9, 10). An emerging alternative that can provide nongenetic, instantaneous, and spatial control is photothermal stimulation using Au- and Si-based nanomaterials (11–14). Although this approach can provide light-based control similar to optogenetics (with subcellular precision), it has limitations, including the need for relatively high laser power, low photothermal conversion efficiency, low absorption cross-section, and limited long-term stability when a stable interface is needed (15, 16).

Two-dimensional (2D) cell culture has been foundational for in vitro research of cellular communication (17, 18). However, its use for disease modeling and designing of new therapeutic interventions has been limited due to its challenge in portraying a native 3D tissue microenvironment (19–22). The 3D tissues, such as spheroids and organoids, have opened new opportunities to develop in vitro models that better mimic in vivo physiology and have enabled new ways to study disease pathology (23, 24). New technologies are needed in order to understand the mechanisms underlying cell–cell communication and the interplay between different cell populations in health and disease. Therefore, there is a need to develop a remote, nongenetic, and minimally invasive modulation of neuronal activity in 3D tissues that will enable understanding of cellular physiology in both healthy and diseased states to develop new therapeutic platforms.

Here, we resolve the limitations of the current state-of-the-art platforms with a complementary approach based on a hybrid nanomaterial composed of 3D out-of-plane fuzzy graphene grown on an intrinsic Si nanowire (i-SiNW) template. The high

Significance

Modulation of cellular electrophysiology helps develop an understanding of cellular development and function in healthy and diseased states. We modulate the electrophysiology of neuronal cells in two-dimensional (2D) and 3D assemblies with subcellular precision via photothermal stimulation using a multiscale fuzzy graphene nanostructure. Nanowire (NW)-templated 3D fuzzy graphene (NT-3DFG) nanostructures enable remote, nongenetic photothermal stimulation with laser energies as low as subhundred nanojoules without generating cellular stress. NT-3DFG serves as a powerful toolset for studies of cell signaling within and between in vitro 3D models (human-based organoids and spheroids) and can enable therapeutic interventions.

Author contributions: T.C.-K. designed research; S.K.R., R.G., M.G.S., B.I.P., J.E.H., S.K., C.G.E.M., and N.J. performed research; S.K.R., R.G., M.G.S., B.I.P., J.E.H., S.K., C.G.E.M., N.J., D.S.R., F.B., J.F.C., M.S.G., M.C., and T.C.-K. analyzed data and discussed results; and S.K.R., R.G., and T.C.-K. wrote the paper.

The authors declare no competing interest.

This article is a PNAS Direct Submission.

Data deposition: All data related to the presented figures are available through Carnegie Mellon University research repository (Kilthub) at doi.org/10.1184/R1/c.4943241.v1.

[1]S.K.R. and R.G. contributed equally to this work.

[2]To whom correspondence may be addressed. Email: tzahi@andrew.cmu.edu.

This article contains supporting information online at https://www.pnas.org/lookup/suppl/doi:10.1073/pnas.1919921117/-/DCSupplemental.

First published June 1, 2020.

photothermal efficiency and subcellular dimensions of nanowire-templated 3D fuzzy graphene (NT-3DFG) (25) enable instantaneous, remote, and nongenetic photothermal stimulation of cells at subcellular spatial resolution using significantly lower laser energies, that is, one to two orders of magnitude lower than other optical platforms. NT-3DFG's high broadband absorbance spectrum provides flexibility to modulate neuronal behavior with different excitation wavelengths. The ease with which the surface chemistry of NT-3DFG can be tuned via chemical or peptide-based functionalization enables stable biointerfaces. This allows us to modulate the neuronal activity in both 2D neuronal cultures and 3D neural spheroids, toward an understanding of cellular physiology, with the long-term goal of applications in intact tissues.

Results

Highly Controlled Out-of-Plane Growth of Single- to Few-Layer 3D Graphene on an SiNW. Previously, we demonstrated synthesis of NT-3DFG mesh composed of 3D out-of-plane single- to few-layer graphene flakes grown on an interconnected SiNW mesh template (25). Here, we isolate individual NT-3DFG to achieve subcellular interfaces with neurons (Fig. 1*A*). The out-of-plane morphology of graphene flakes from the i-SiNW core, illustrated in Fig. 1*A*, was confirmed by scanning electron microscopy (SEM) and high-resolution transmission electron microscopy (HR-TEM) imaging (Fig. 1 *B* and *C* and *SI Appendix*, Figs. S1 and S2). The presence of single- to few-layer graphene flakes was confirmed by HR-TEM (Fig. 1*D* and *SI Appendix*, Fig. S2) and Raman spectroscopy (for detailed Raman characterization and analysis, see *SI Appendix*). The intricate architecture of out-of-plane graphene flakes forms a polycrystalline network (Fig. 1 *D*, *Inset*) (26). The interplanar distances for the first and second nearest C–C neighbors are experimentally derived to be 0.123 and 0.212 nm, respectively (*SI Appendix*, Table S3). These values agree with the expected interplanar spacing for the $(11\bar{2}0)$ plane ($d_{11\bar{2}0}$ = 0.123 nm) and the $(10\bar{1}0)$ plane ($d_{10\bar{1}0}$ = 0.213 nm) (25, 27). The distance between individual graphene layers, calculated using the (0002) reflection in the diffraction pattern (*SI Appendix*, Table S3) and interplanar fringe intensities in the HR-TEM image (*SI Appendix*, Fig. S2), was determined to be 0.36 and 0.37 nm, respectively. These values are greater than the interlayer distance of bulk graphite (0.344 nm), corroborating the presence of turbostratic graphene (25, 26, 28, 29).

NT-3DFG Exposed Graphene Surface as a Platform for Chemical Modifications. We have previously demonstrated that the out-of-plane synthesis of graphene flakes results in an enormous available surface area (25). In addition, graphene flakes provide the opportunity for surface functionalization via $\pi-\pi$ interactions or covalent bonding (30, 31). Directed self-assembly of a polypeptide (31) can control the surface charge of the graphene, hence maximizing NT-3DFG electrostatic attachment to the cell membrane. To create stable aqueous suspensions and increase cell membrane adhesion, graphene flakes were treated with HNO_3 and functionalized with lysine-phenylalanine based peptide $(KF)_4$ (30, 31), as confirmed by X-ray photoelectron spectroscopy (XPS) characterization (for detailed XPS characterization, see *SI Appendix*).

High Photothermal Efficiency of NT-3DFG. Bottom-up synthesis of NT-3DFG allows us to tailor the 3DFG flake size and density by changing the synthesis time (*SI Appendix*, Fig. S5*A*). Changing the physical architecture of NT-3DFG by increasing the 3DFG flake size and density leads to an increase in the absorbance in the ultraviolet visible (UV-Vis) regime (*SI Appendix*, Fig. S5 *B* and *C*). The UV-Vis spectrum for i-SiNW agrees well with previously reported results (32–34). The enhanced broadband absorption by NT-3DFG can be attributed to the increased light trapping by the densely packed out-of-plane 3DFG flakes, as this structure is synonymous to that of nanostructured silicon and carbon metamaterials (35–37). Due to its high broadband absorption, that is, UV to near-IR (NIR), of *ca*. 95%, NT-3DFG synthesized for 90 min was selected for subsequent characterization. At a single-nanowire level, we observe that the addition of out-of-plane 3D graphene architecture along an i-SiNW leads to a fourfold to fivefold increase in the extinction spectrum (Fig. 2*A*). We note that the full width at half maximum (FWHM) of the elliptical laser spot used for the single-nanowire extinction measurements (5 μm × 8 μm) is much larger than the diameter of NT-3DFG (see *Materials and Methods* for details regarding the UV-Vis and single-nanowire extinction spectroscopy). This results in the measured extinction magnitude being a lower limit to the actual material property. The broadband absorption across visible and NIR spectrum by single NT-3DFG is further corroborated by the extinction measurements. The ability to use NIR is crucial for translation to in vivo studies because it enables an increase in tissue penetration depth due to reduced absorption by water and hemoglobin (38).

Absorption of light energy by materials can lead to the generation of thermal energy (via photothermal effects) (11, 12, 39–41) and/or the accumulation of charge carriers (via photoelectric effects) (14, 42). In the case of NT-3DFG, we observe a dominant photothermal effect. This was quantified by measuring the effective local temperature change in the vicinity of isolated NT-3DFG under laser illumination using a micropipette resistance method (39), as illustrated in *SI Appendix*, Fig. S7 (for more details, see *Materials and Methods*). For a representative isolated NT-3DFG, the local temperature change increases from 1.86 ± 0.03 K to 6.74 ± 0.07 K with increase in laser power from 2 mW to 10 mW (635-nm laser with a 20-μm spot size and 1-ms pulse width) (Fig. 2*B*). NT-3DFG is a broadband absorber; thus any laser wavelength pulses can be used to induce a local temperature change. We demonstrate this by measuring the local

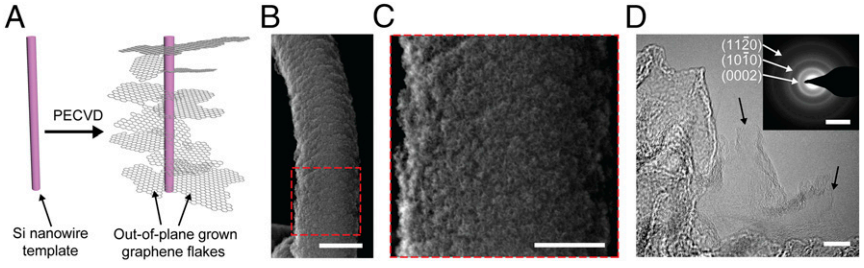

Fig. 1. Highly controlled out-of-plane growth of single- to few-layer 3D graphene flakes on an SiNW. (*A*) Schematics of NT-3DFG. (*B*) SEM image of NT-3DFG. (Scale bar, 1 μm.) (*C*) Expanded view of the marked red dashed box in *B*. (Scale bar, 500 nm.) (*D*) HR-TEM image of NT-3DFG. Black arrows indicate single-layer graphene flakes. (Scale bar, 10 nm.) *Inset* is a representative selected area electron diffraction (SAED) pattern of NT-3DFG. (Scale bar, 5 nm^{-1}.)

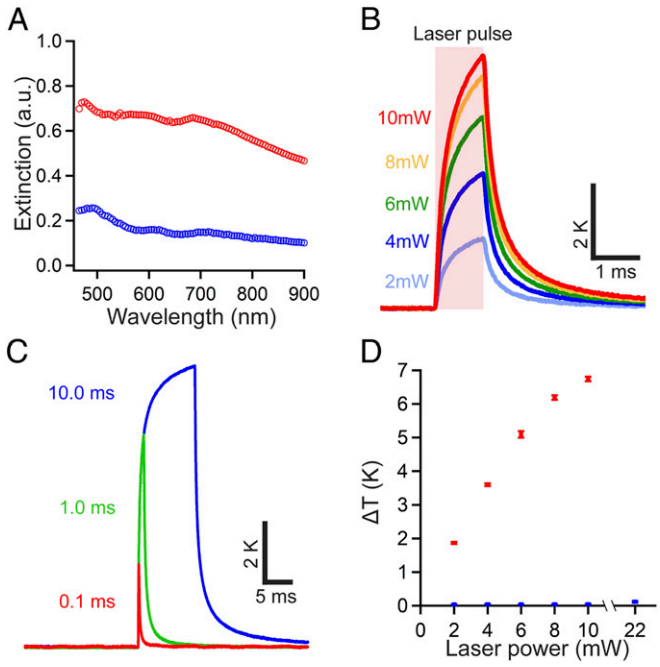

Fig. 2. NT-3DFG is a photothermally active hybrid nanomaterial. (*A*) Mean extinction spectra of isolated NT-3DFG (red, $n = 6$) and bare i-SiNW (blue, $n = 4$) as a function of wavelength. (*B*) Temperature change as a function of time for a representative isolated NT-3DFG under varying powers of the incident laser (635-nm laser, 20-μm spot size, 1-ms pulse width). Results are presented as average of 10 individual pulses. The shaded region represents the duration of the laser pulse. (*C*) Temperature change as a function of time for a representative isolated NT-3DFG under varying pulse durations of the incident laser (635-nm laser, 20-μm spot size, 10-mW power). Temperature change values were averaged from 10 individual pulses. (*D*) Temperature change as a function of power of the incident laser (635-nm laser, 20-μm spot size, 1-ms pulse width) for a representative isolated NT-3DFG (red, representative of 9 independent NT-3DFG) and a representative isolated bare i-SiNW (blue, representative of 10 independent i-SiNWs). Results are presented as mean ± SD ($n = 10$ measurements per wire).

temperature change induced by different laser wavelengths, i.e. 405 nm (*SI Appendix*, Fig. S8 and Tables S7 and S8).

The local temperature change can be further regulated by modulating the duration of the illuminating laser pulses at constant power. Under constant laser intensity (10 mW), reducing the laser pulse duration from 10.0 ms to 0.1 ms reduces the maximal temperature change (ΔT) from 8.89 ± 0.07 K to 2.61 ± 0.04 K (Fig. 2*C*). However, the average rate of change in the temperature ($\Delta T/\Delta t$) drastically increases from 5,000 K/s to 20,000 K/s (for details on calculations, see *Materials and Methods*). The increase in temperature of NT-3DFG, when a 1-ms pulse of 2-mW or 10-mW laser is applied, is ∼140- and 260-fold, respectively, higher than that observed with the application of the same laser pulses to bare i-SiNWs (Fig. 2*D* and *SI Appendix*, Fig. S9 and Tables S6–S10). We attribute the enhanced photothermal performance of NT-3DFG to its high UV-Vis absorbance; it will necessitate future studies to elucidate the mechanism for this behavior. Similar temperature changes have been demonstrated for either Au- or Si-based nanomaterials, but only with laser power densities one to two orders of magnitude higher than those used on NT-3DFG [e.g., 240 kW/cm^2 for Si-based nanomaterials (12, 14), and 31 kW/cm^2 for Au nanoparticles (11) as compared to 1 kW/cm^2 to 3 kW/cm^2 for NT-3DFG].

Neuron and NT-3DFG Interaction. Previously, photothermal effects have been demonstrated to induce changes in cell membrane capacitance, eliciting an action potential in excitable cells (11, 12, 14, 39–41). The high photothermal efficiency of NT-3DFG makes it a promising nanomaterial to enable stimulation with significantly lower laser energies. Prior to employing NT-3DFG for photothermal stimulation of neurons, it is critical to assess the cytotoxicity of NT-3DFG as well as identify the interface between NT-3DFG and target neurons. We synthesized NT-3DFG suspensions with an average length of *ca*. 7.32 μm (*SI Appendix*, Fig. S10) and incubated varying concentrations of the suspension with primary rat dorsal root ganglion (DRG) neurons (for details, see *Materials and Methods*). As the NT-3DFG concentration is increased from 0.15 ± 0.01 μg/mL to 0.75 ± 0.05 μg/mL, the density of NT-3DFG also increases from 257 ± 56 wires/mm^2 to 565 ± 104 wires/mm^2 (*SI Appendix*, Fig. S11 and Table S12). Consequently, the density of cells interfaced with NT-3DFG also increased from 104 ± 19 cells/mm^2 (i.e., 19 ± 8% of total cells) to 179 ± 20 cells/mm^2 (i.e., 45 ± 14% of total cells) (*SI Appendix*, Fig. S11 and Table S12). We note that NT-3DFG concentration of 0.15 ± 0.01 μg/mL has no significant effect on the viability of neurons after 24 h of incubation (*SI Appendix*, Fig. S12). Increasing the NT-3DFG concentration to 0.75 ± 0.05 μg/mL leads to a decrease in viability from 94 ± 4% to 88 ± 5% (*SI Appendix*, Fig. S12). This observation is in line with the effect of increasing nanoparticle concentration on cell viability for various nanoparticles (43–45).

After incubating DRG neuron cell cultures with NT-3DFG for 24 h, we observe that NT-3DFG adhere to the plasma membrane rather than getting internalized by the cells. This is highlighted by the 3D reconstruction, orthogonal sections, and SEM images of the interface between DRG neurons and NT-3DFG presented in Fig. 3 and *SI Appendix*, Fig. S13. We attribute the adhesion between plasma membrane and NT-3DFG to the polypeptide surface functionalization of NT-3DFG. Thus, the high photothermal performance, minimal cytotoxicity, and noninvasiveness

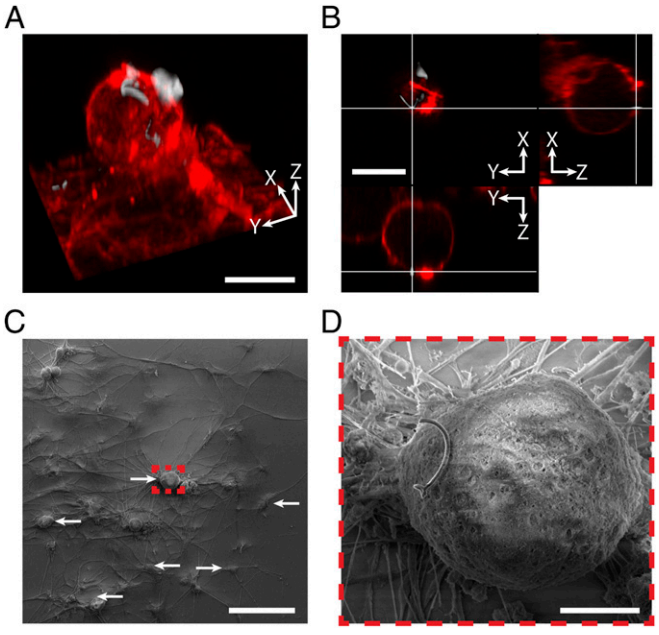

Fig. 3. NT-3DFG adhere to the cell membrane of DRG neurons. (*A*) A 3D reconstruction of a fluorescent images of a representative DRG neuron labeled with plasma membrane stain (red, CellMask plasma membrane stain) and interfaced with NT-3DFG (white). (Scale bar, 20 μm.) (*B*) Orthogonal sections of the DRG neuron presented in *A*. (Scale bar, 20 μm.) (*C*) Representative SEM image of DRG neurons incubated with NT-3DFG for 24 h. White arrows indicate NT-3DFG interfaced with DRG neurons and glial cells. (Scale bar, 100 μm.) (*D*) Expanded view of the marked red dashed box in *C*. (Scale bar, 10 μm.)

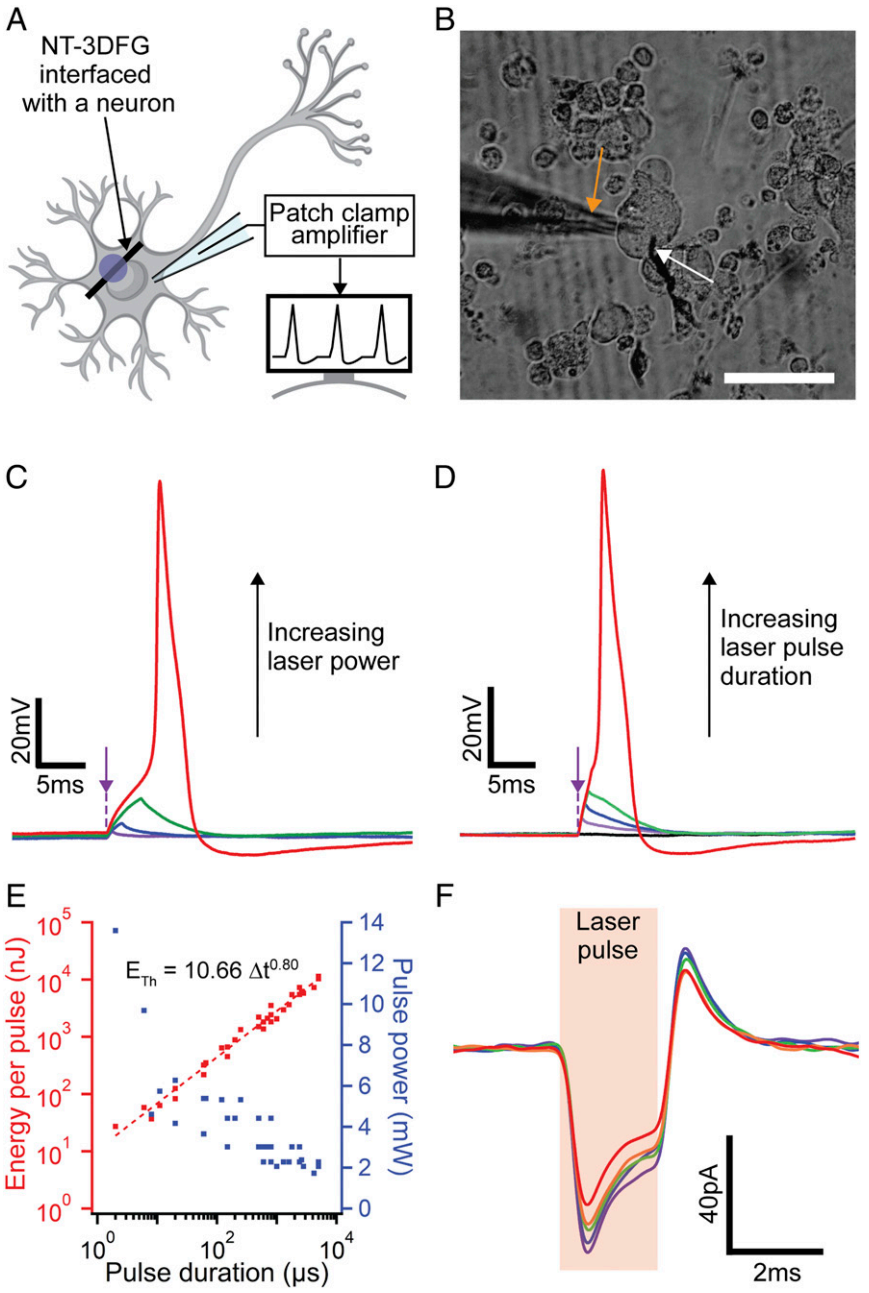

Fig. 4. Remote nongenetic optical modulation of neuronal activity with high precision and low laser energy. (*A*) Schematic illustrating a NT-3DFG interfaced with a neuron for photothermal stimulation. Purple spot indicates laser illumination area. (*B*) Bright-field image of a DRG neuron interfaced with an NT-3DFG. Orange and white arrows indicate the patch pipette and the laser pulse illumination point, respectively. (Scale bar, 50 μm.) (*C*) Representative recorded DRG neuron membrane potential using patch clamp in current clamp mode. The DRG neuron was illuminated by a 405-nm laser with 1.2-ms pulse duration and varying powers of 1.45 mW (1.74 μJ, violet), 1.73 mW (2.08 μJ, blue), 2.28 mW (2.73 μJ, green), and 3.02 mW (3.62 μJ, red). Purple arrow indicates the applied laser pulse starting point. (*D*) Representative recorded DRG neuron membrane potential using patch clamp in current clamp mode. The DRG neuron was illuminated by a 405-nm laser of 2.28-mW power and varying pulse durations of 0 ms (0 μJ, black), 0.4 ms (0.91 μJ, violet), 0.8 ms (1.82 μJ, blue), 1.2 ms (2.74 μJ, green), and 1.6 ms (3.65 μJ, red). Purple arrow indicates the applied laser pulse starting point. (*E*) Laser energy per pulse and pulse power required for photothermal stimulation of neurons as a function of laser pulse duration ($n = 12$ DRG neurons). Dashed red line is a power-law fit between threshold energy required for stimulation (E_{Th}) and the duration of the laser pulse (Δt); $E_{Th} = 10.66 * \Delta t^{0.80}$. (*F*) Representative recorded capacitive current transients in response to laser pulses with pulse duration of 2 ms and laser power of 1.73 mW (3.46 μJ). Neurons were patch-clamped in whole-cell configuration and voltage clamp mode with holding potentials of −150 (violet), −140 (blue), −130 (green), −120 (orange), and −110 (red) mV ($n = 3$ DRG neurons).

of NT-3DFG establish it as an ideal candidate for targeted photothermal stimulation of neuronal cells.

Modulation of Neuronal Electrical Activity Using NT-3DFG. To investigate the remote, nongenetic, optical modulation of neuronal activity capabilities of NT-3DFG, the interface between NT-3DFG and DRG neuron plasma membrane was illuminated with laser pulses, as illustrated in Fig. 4*A* (for details, see *Materials and Methods*). The significantly smaller diameter of NT-3DFG (1.4 ± 0.1 μm) compared to the neuronal body (10 μm to 50 μm) enables high precision and subcellular spatial resolution (Fig. 4*B*). Illuminating the cell–NT-3DFG interface with laser

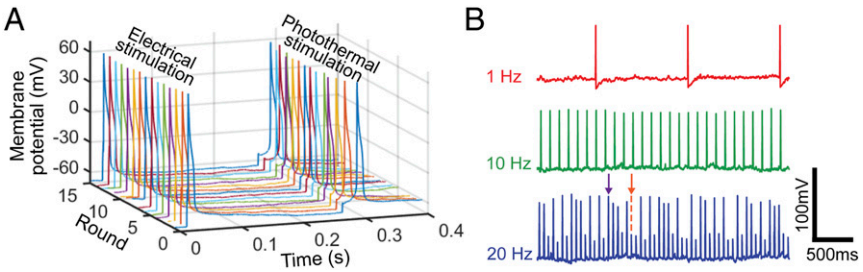

Fig. 5. Highly controlled photothermal stimulation of neurons. (*A*) Representative recorded membrane potential of a repetitively stimulated DRG neuron (DRG neuron was patch-clamped in whole-cell configuration and current clamp mode). Electrical stimulation was performed by injecting a pulse of 100 nA for 1 ms. Photothermal stimulation was performed with 405-nm laser with pulse of 2.28-mW power and 0.6-ms pulse duration (1.37 μJ). (*B*) Representative recorded membrane potential of a DRG neuron exposed to trains of laser pulses at different frequencies ($n = 3$ DRG neurons). A 405-nm laser with pulse of 3.02-mW power and 0.7-ms pulse duration (2.11 μJ) was used (DRG neuron was patch-clamped in whole-cell configuration and current clamp mode). Purple and orange arrows indicate an action potential and a subthreshold depolarization, respectively.

pulses leads to depolarization of the cell membrane, as observed in the patch clamp measurements (Fig. 4 *C* and *D*). The membrane potential was progressively depolarized with increasing laser energy, either by increasing the laser power from 1.45 mW to 3.02 mW while keeping pulse duration fixed at 1.2 ms (Fig. 4*C*) or by increasing the laser pulse duration from 0.4 ms to 1.6 ms while keeping the laser power fixed at 2.28 mW (Fig. 4*D*). Laser energy of *ca*. 3.6 μJ per pulse induced enough depolarization of the cell membrane to reach the action potential threshold. The absence of any depolarization upon illumination of the cell away from the NT-3DFG confirms that the stimulation occurred due to photothermal effect of the NT-3DFG (*SI Appendix*, Fig. S15). The high photothermal efficiency of NT-3DFG enables stimulation of neurons with laser energies fivefold to 60-fold lower than what has been reported previously using other nanomaterials (11–14).

The mechanism of photothermal stimulation via NT-3DFG follows optocapacitive stimulation, that is, photothermal stimulation of cells due to changes in membrane capacitance. The rate of change in temperature at the cell membrane (dT/dt) is proportional to the rate of change of membrane capacitance (dC_m/dt), resulting in a capacitive current (I_c) (46). The greater the magnitude of I_c, the more easily an action potential is evoked. As long as the magnitude of instantaneous dT/dt is large

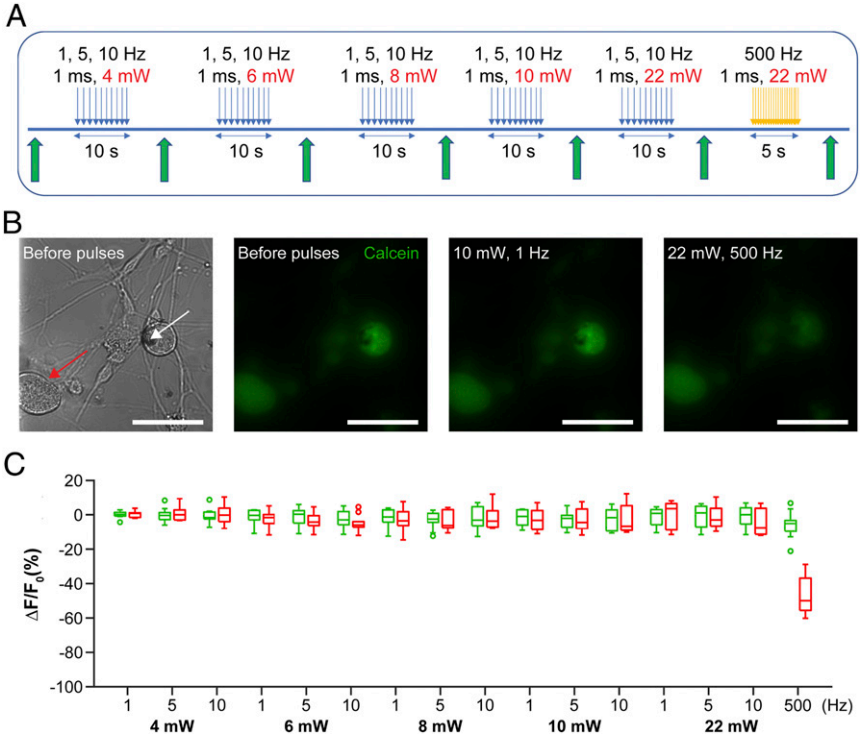

Fig. 6. Photothermal stimulation with NT-3DFG does not affect cellular viability. (*A*) Schematic illustrating the experimental design of the viability assay performed on the Calcein loaded DRG neurons before and after the application of laser pulses. Blue arrows indicate illumination by 635-nm laser with 1-ms pulse duration and varying powers of 4 mW (4 μJ), 6 mW (6 μJ), 8 mW (8 μJ), 10 mW (10 μJ), and 22 mW (22 μJ), at varying frequencies (1, 5, and 10 Hz). Orange arrows indicate pulse train of 2,500 pulses of 1-ms pulse duration at 500 Hz. Green arrows indicate acquisition of images using blue laser and GFP filter. (*B*) Bright-field and fluorescence images of Calcein loaded DRG neurons before and after laser pulses. White arrow indicates the NT-3DFG illuminated by the laser. Red arrow indicates a neighboring cell without laser illumination. (Scale bars, 50 μm.) (*C*) Box plot presenting the change in fluorescence of targeted cells (green) and neighboring cells (red) as a function of laser pulse condition ($n = 10$ DRG neurons). Empty circles indicate outliers in the respective data sets.

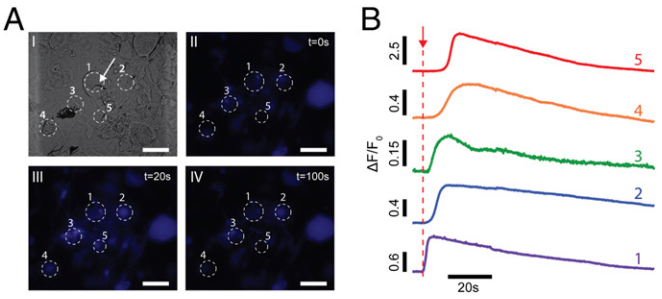

Fig. 7. Photothermal stimulation of a 2D DRG network. (*A*) Representative bright-field (I) and time series fluorescent images (II to IV) of cells loaded with calcium indicator dye (Cal 520). A 635-nm laser with pulse of 4-mW power and 1-ms pulse duration (4 μJ) was applied at $t = 5$ s. White arrow indicates the NT-3DFG illuminated by the laser pulse. (Scale bars, 50 μm.) (*B*) Normalized calcium fluorescence intensity curves of the cells marked in *A*. Red arrow represents the applied laser pulse starting point ($t = 5$ s).

enough to generate I_c greater than the necessary threshold, an action potential will be elicited irrespective of the total duration of the laser pulse. Therefore, shorter pulses are more energetically efficient at triggering an action potential. The thermal energy output of longer pulses beyond the threshold point does not contribute toward triggering an action potential (Fig. 2*C*) (40). By applying laser pulses of sub-10-μs pulse duration, we were able to further reduce the energy required to reach the action potential threshold to sub-100 nJ per pulse. With NT-3DFG, we were able to reduce the pulse duration from 1 ms (2.7-mW laser power, 2.7-μJ laser energy) to 2 μs (10-mW laser power, 20-nJ laser energy) and still elicit an action potential (Fig. 4*E* and *SI Appendix*, Fig. S16 and Table S13). Although the 500-fold decrease in laser pulse duration required a fourfold increase in laser power to reach the threshold energy, the effective energy input to elicit an action potential reduced by more than 100-fold (Fig. 4*E* and *SI Appendix*, Table S13).

For optocapacitive stimulation, the energy needed to reach the action potential threshold (E_{Th}) and the laser pulse duration (Δt) follow a power-law relationship (40). We observe a similar power-law relationship for NT-3DFG–based photothermal stimulation (Fig. 4*E*), corroborating the role of an optocapacitive mechanism in photothermal stimulation via NT-3DFG. The magnitude of the prefactor coefficient (10.66) of the E_{Th} *vs.* Δt fit reveals a 2.5- to 10-fold lower energy requirement to reach threshold membrane potential to stimulate a cell in comparison to Au, carbon nanotube mesh, and other graphite-based nanomaterials (40). Additional membrane voltage measurements were performed with holding potentials ≤ −110 mV to prevent the activation of voltage-gated ion channels. The generation of transient inward currents upon laser illumination of the NT-3DFG–neuron interface (Fig. 4*F*) further corroborates the optocapacitive nature of the stimulation (41).

To investigate the reproducibility of the photothermal stimulation technique, the NT-3DFG–cell interface was repetitively illuminated with laser pulses. Fig. 5*A* demonstrates the response of a patch-clamped neuron upon electrical stimulation (left spikes) followed by photothermal stimulation using a 405-nm laser (right spikes). The neuron elicited an action potential in response to every stimulus application, showing high reproducibility. Furthermore, the laser pulses were applied with varying frequencies of 1, 10, and 20 Hz for 10 s each. Neurons were able to reliably follow pulse trains with frequencies up to 10 Hz (Fig. 5*B*). However, there were action potential failures at 20-Hz stimulation (Fig. 5*B*, orange arrow). This is likely to reflect the intrinsic properties of DRG neurons (i.e., the ion channels underlying spike initiation), given that nociceptive neurons, those with action potential shapes similar to those shown in Fig. 5*B* (47, 48), rarely fire at frequencies above 3 Hz (49). This assay confirms that NT-3DFG enables highly controlled and reproducible remote modulation of neuronal activity at subcellular precision.

Effect of Photothermal Stimulation on Cell Viability. To evaluate the effect of photothermal stimulation on cellular viability, we investigated the power threshold at which viability was impacted. DRG neurons, loaded with Calcein, a live cell indicator dye, were interfaced with NT-3DFG. Then 1-ms laser pulses of varying laser power and pulse frequency ranging from 4 mW to 22 mW and 1 Hz to 10 Hz, respectively, were applied to the cell–nanowire interface (Fig. 6*A*). The cells were imaged before and after the laser pulses (Fig. 6*B*) (details can be found in *Materials and Methods*). No significant change in fluorescence intensity was observed for laser pulses applied at 1 Hz to 10 Hz for 10 s with laser powers of 4 mW (4 μJ per pulse) to 22 mW (22 μJ per pulse) (Fig. 6*C*). Cells that were exposed to 500-Hz pulse trains of 1-ms pulses for 5 s with 22-mW laser power (2,500 pulses of 22 μJ every 2 ms) exhibited a significant loss in fluorescence (Fig. 6 *B* and *C*). At higher laser powers, the local change in temperature induced by NT-3DFG is higher. Under the extreme stimulation conditions of 22 mW and 500 Hz, the change in temperature experienced by the plasma membrane will be much greater than that under safe photothermal stimulation conditions. Extreme change in local temperature is expected to damage the plasma membrane (50). Therefore, we attribute the loss in fluorescence under extreme stimulation conditions to cell death as a result of damage to the plasma membrane. We note that neighboring cells did not show a change in fluorescence, indicating that the fluorescence change of the cell under stimulation was not due to photobleaching of the dye. The maximum energy used for photothermal stimulation of neurons was *ca.* 3 μJ, significantly lower than the energy needed to damage the cells, thus confirming that there were no toxic effects of the NT-3DFG–based photothermal stimulation platform.

Multicell Dynamics via Calcium Imaging. To demonstrate the capability of modulating neuronal activity at a network scale with subcellular precision, NT-3DFGs were interfaced with neuronal networks, and multicell dynamics were investigated upon photothermal stimulation using calcium imaging. Calcium is a ubiquitous secondary messenger that plays an essential role in the signal transduction of excitable cells (51). Calcium ions enter the excitable cells during an action potential firing; therefore, changes in intracellular calcium can be used as a proxy for

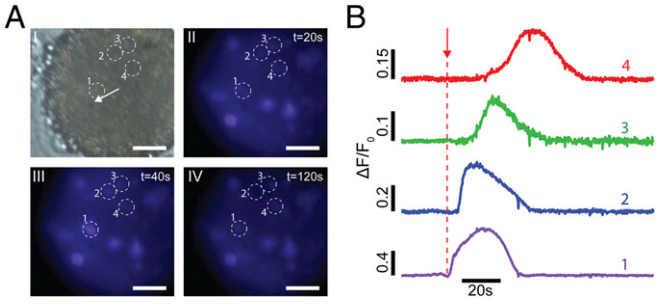

Fig. 8. Photothermal stimulation of 3D cortical spheroids. (*A*) Representative bright-field (I) and time series fluorescent images (II to IV) of a cortical spheroid loaded with calcium indicator dye (Cal 520). A 635-nm laser with pulse of 6-mW power and 1-ms pulse duration (6 μJ) was applied at $t = 25$ s. White arrow represents the NT-3DFG illuminated by the laser pulse. (Scale bars, 50 μm.) (*B*) Normalized calcium fluorescence intensity curves of the cells marked in *A*. Red arrow represents the applied laser pulse starting point ($t = 25$ s).

electrical activity (51). To evaluate the effect of photothermal stimulation on the calcium dynamics of DRG neurons, NT-3DFGs were interfaced with cells loaded with calcium indicator dye, Cal 520. Illumination of the NT-3DFG with a laser pulse of 4-mW power and 1-ms pulse width led to an influx of calcium, as evident from the increase in fluorescence (Fig. 7 and *SI Appendix*, Fig. S17). Furthermore, the stimulation led to the propagation of the calcium transient from the stimulated cell to the neighboring cells as observed by the delay in the fluorescence change response of the neighboring cells (Fig. 7 and Movie S1). The propagation of the calcium transients is attributed to the presence of intercellular junctions and diffusion of chemical messengers (12, 14, 52–54). As a control experiment, we illuminated cells away from the NT-3DFG site using the same conditions for the laser pulses and observed no change in fluorescence, confirming the high spatial precision of the photothermal stimulation (*SI Appendix*, Fig. S18).

Our remote nongenetic photothermal stimulation can be easily implemented in a 3D cellular organization such as cellular spheroids or organoids. The inability of 2D cell culture models to recapitulate in vivo-like cytoarchitectural organization and intercellular connections has impeded their use, especially for disease modeling and designing new therapeutic interventions (19, 20, 55). Complex 3D arrangement of cells, such as spheroids and organoids, better represents in vivo-like behavior in terms of morphology (56), cell survival (57), and electrophysiological characteristics (58). However, there is a need to develop a nongenetic, remote, minimally invasive, and biocompatible platform that can allow precise modulation of the neuronal activity in 3D systems to better understand cellular physiology of both healthy and diseased states, for developing new therapeutics.

As a proof of concept, we demonstrate the capability to interface NT-3DFGs with 3D cortical neural spheroids. NT-3DFG can be conformally distributed throughout the periphery and bulk of cortical spheroids simply by incubating the target spheroid(s) with NT-3DFG suspension (*SI Appendix*, Figs. S19 and S20). Our simple approach of interfacing NT-3DFG with 3D neural spheroids allows us to interface isolated NT-3DFG with individual neuronal cells. Illuminating the interface between individual NT-3DFG and cortical neurons in the spheroids with laser pulses of 4- to 6-mW power and 1-ms pulse width leads to an influx of calcium in the neuronal networks, as observed by changes in the fluorescence intensity of the cells (Fig. 8, *SI Appendix*, Fig. S21, and Movie S2). The duration and shape of the calcium transients observed in the neural spheroids upon photothermal stimulation are in line with reported literature (59, 60). Illumination of cells away from the NT-3DFG result in no observable change in the fluorescence emission, further confirming the spatial precision of the photothermal stimulation in a 3D cellular arrangement (*SI Appendix*, Fig. S22). This work demonstrates the ability to stimulate and modulate activity of 3D neural spheroids noninvasively with high precision.

Discussion

In this study, we demonstrate a hybrid nanomaterial composed of 3D fuzzy graphene grown on an i-SiNW template for remote, nongenetic optical modulation of neuronal activity in both in two and three dimensions, at a single-cell level. Presence of graphene allows straightforward surface modifications using both chemical treatments and peptide coatings. The unique structure of this hybrid nanomaterial leads to extraordinary optical and photothermal properties that enable stimulation of neurons with laser energies as low as subhundred nanojoules, one to two orders of magnitude lower than Au-, C-, and Si-based photostimulation (11–14). The <1.5-μm diameter of NT-3DFG allows stimulation with high precision and subcellular spatial resolution. Moreover, the ability of NT-3DFG to absorb light in the NIR regime will be crucial for modulation of neuronal activity in an in vivo model (38). The NT-3DFG platform will greatly impact our basic understanding of cellular communication across various electrically active cells (such as neurons and myocytes) and tissues in both health and disease. In addition to basic research, this technology will allow development of therapeutic interventions for a variety of diseases resulting in problems such as muscle loss, chronic pain, and neurodegeneration. The ability to modulate activity of neural spheroids opens up unique opportunities to use spheroids and organoids as model systems for therapy development for various neurodegenerative disorders, such as Parkinson's disease. Moreover, this platform can be adapted to address challenges in tissue engineering by enabling noninvasive high-precision stimulation control of engineered tissues (61).

Materials and Methods

Synthesis of NT-3DFG. NT-3DFG is synthesized via a two-step process: i-SiNWs synthesis, followed by 3DFG synthesis. The i-SiNWs were synthesized through Au nanoparticle (AuNP)-catalyzed vapor–liquid–solid growth process (25). A 2.0 cm × 2.0 cm (100) Si substrate with 600-nm wet thermal oxide (p-type, ≤0.005 Ω cm, Nova Electronic Materials Ltd., catalog no. CP02 11208-OX) or 1.5 cm × 1.5 cm fused silica (University Wafer, catalog no. 1013) substrates were cleaned with acetone and isopropyl alcohol (IPA) in an ultrasonic bath for 5 min each followed by N_2 blow dry. The substrate was then treated with UV ozone (PSD Pro series digital UV-Ozone, Novascan) at 150 °C for 10 min. Cleaned substrates were then functionalized with 500 μL of 4:1 deionized (DI) water:poly-L-lysine (PLL) (0.1% wt/vol, Sigma-Aldrich, catalog no. P8920) for 8 min. They were then gently cleaned three times in DI water and N_2 blow-dried. Then, 500 μL of 9:1 DI water:30 nm AuNP solution (Ted Pella, catalog no. 15706-1) was dispersed onto the PLL-coated substrate for 8 min. The substrate was then gently washed three times in DI water and N_2 blow-dried. AuNP functionalized substrates were then introduced into a custom-built chemical vapor deposition (CVD) setup. Once a baseline pressure of 1×10^{-5} Torr was reached, the temperature was ramped up to 450 °C in 8 min, which was followed by a 5-min temperature stabilization step. Nucleation was conducted at 450 °C for 15 min under 80 standard cubic centimeters per minute (sccm) H_2 (Matheson Gas) and 20 sccm SiH_4 (10% in H_2, Matheson Gas) at a controlled pressure of 40 Torr. The synthesis step was performed at 450 °C for 100 min under 80 sccm H_2 and 20 sccm SiH_4 at a controlled pressure of 40 Torr. The sample was cooled down to room temperature at base pressure post-synthesis.

The 3DFG was synthesized through plasma-enhanced CVD (PECVD) process (25). Post i-SiNW synthesis, the sample was introduced into a custom-built PECVD setup. The synthesis process was carried out at 800 °C and at a total pressure of 0.5 Torr. The SiNWs sample was placed 4.0 cm from the edge of the radio frequency (RF) coil and out of the PECVD furnace. The temperature of the furnace was ramped up to the synthesis temperature at 55 °C·min^{-1}, which was followed by a temperature stabilization step at the synthesis temperature for 5 min, under a flow of 100 sccm Ar (Matheson Gas). Prior to the synthesis step, inductively coupled plasma was generated using a 13.56-MHz RF power supply (AG 0313 Generator and AIT-600 RF, power supply and auto tuner, respectively, T&C Power Conversion, Inc.) with the plasma power constant at 50 W; the furnace was moved over the sample following plasma ignition. The synthesis step was conducted under 50 sccm CH_4 precursor (5% CH_4 in Ar, Airgas) for 5, 10, 30, or 90 min. The plasma was turned off after the synthesis step, and the sample was rapidly cooled from growth temperature to 100 °C in 30 min under the flow of 100 sccm Ar (62).

NT-3DFG Sample Preparation for Structural, Optical, and Photothermal Characterizations. A 5 mm × 5 mm sample of NT-3DFG was cleaved from the center of the growth substrate and placed in a clean 2-mL scintillation vial. Then, 100 μL of IPA was added to the vial. The vial was placed in an ultrasonic bath (Crest Ultrasonics, catalog no. P230D) at 45 kHz and 32 W for 2 s. Then 5 μL of the suspension was drop-casted onto Si/SiO_2 or glass substrates, and the IPA was allowed to dry in the clean hood. The samples were kept on the hot plate at 60 °C for 15 min.

SEM. SEM imaging was performed using an FEI Quanta 600 field emission gun SEM. Images were acquired at accelerating voltages of 2 kV to 20 kV with a working distance of 5 mm. For imaging of isolated NT-3DFGs, NT-3DFGs were drop-casted on indium tin oxide-coated polyethylene terephthalate films. No additional conductive coating was applied to any samples to assist with imaging.

NT-3DFG diameter was quantified from the high-resolution (2,048 × 1,768 pixels) SEM images using ImageJ (Java-based open-source image processing software, NIH). Quantification was performed on 150 wires across three independent samples.

HR-TEM. HR-TEM imaging was performed using an FEI Titan G2 80-300 Cs corrected TEM fitted with a high-resolution Gatan Imaging Filter Tridiem energy filter. A lacey carbon, 300-mesh Cu TEM grid (Ted Pella, catalog no. 01895) was gently rubbed over an NT-3DFG growth substrate. HR-TEM and selected area electron diffraction (SAED) images were acquired at an accelerating voltage of 300 kV with 2,048 × 2,048 slow-scan charge coupled device (CCD) camera. SAED plane spacing analysis and fringe intensity cross-section profiles were quantified from corresponding HR-TEM images using ImageJ (25, 62).

Single-Nanowire Extinction Measurements. Extinction was measured with a supercontinuum laser (NKT Photonics, SuperK Extreme EXB-6) after passing through a monochromator (Princeton Instruments, Acton SP2300) to output a single wavelength with < 2-nm bandwidth. The laser was collimated into a beam size of 1 mm and split evenly into a reference and probe beam for balanced detection with Nirvana balanced photoreceiver (Newport, Nirvana Auto-Balanced Photoreceiver 2007). The probe beam was directed to one side of the back aperture of a reflective objective (Thorlabs, PMM-40×-P01) to deeply underfill the aperture and achieve quasi-plane wave illumination of an isolated NT-3DFG or i-SiNW with a low effective numerical aperture, resulting with an elliptical spot size of *ca*. 8-μm FWHM by 5-μm FWHM. The optical power was collected with the probe beam placed on and off the NT-3DFG by modulating the substrate position using a piezo positioner (Mad City Labs, Nano-LP 200). Measured extinction was calculated as

$$\text{Extinction} = 1 - T,$$

where $T = I/I_0$, and I and I_0 are transmitted powers collected with the beam on and off the NT-3DFG, respectively. Measurements were performed on $n = 6$ for NT-3DFG and $n = 4$ for i-SiNW, and mean spectra were plotted.

Photothermal Characterization. Photothermal characterization was performed using the pipette resistance method (12, 39). A custom-built upright microscope (*SI Appendix*, Figs. S6*A* and S14*A*) with a 40×/0.8 numerical aperture (NA) water immersion objective was used to deliver light pulses from a laser source (405-nm laser, Q-BAIHE; 635-nm laser, NaKu Technology). The laser pulses were controlled by transistor–transistor logic (TTL) signals. Prior to photothermal characterization of NT-3DFG and i-SiNWs, the performance of the 405- and 635-nm lasers was characterized under continuous wave (CW) and pulsing modes of operation. The output power of the laser was measured through the objective using a photodiode power sensor (PM 100D with S121C detector, Thorlabs) under CW operation. A Si amplified photodetector (PDA36A, Thorlabs) was used to measure the output power of the laser under TTL pulsing with pulse widths of 0.1, 1.0, and 10.0 ms. The output voltage of the photodetector was calibrated under CW operation. The output power of laser under TTL pulsing was calculated using the photodetector–laser power calibration curve (*SI Appendix*, Fig. S6*B*).

Voltage clamp measurements were done using a patch clamp amplifier (A-M Systems, Model 2400), controlled by WinWCP software (open source). Glass capillaries with 1.50-mm outer diameter and 0.86-mm inner diameter (Sutter Instrument, catalog no. BF150-86-10) were pulled using a micropipette puller (Sutter Instrument, P-97) for a final resistance of *ca*. 2 MΩ when filled with 1× phosphate-buffered saline (PBS) solution. For nanowire photothermal characterization, bare i-SiNWs or NT-3DFGs were drop-casted on a glass-bottomed dish (MatTek, catalog no. P35G-1.5-14-C). The dish was filled with 4 mL of 1× PBS solution. The temperature of the solution in the Petri dish was continuously measured using a digital thermometer (Signstek, 6802-II). The micropipette tip was positioned in close proximity to the nanowire (*ca*. 2 μm). Ionic currents across the pipette tip and the resistance of the pipette were recorded in the voltage clamp mode. Laser pulses of 0.1, 1.0, and 10.0 ms were applied at varying laser power ranging from 2 mW to 10 mW. A reference electrode (Ag/AgCl) was introduced into the dish.

The change in measured current ($\Delta I_{light}(t)$) post laser illumination can be due to photothermal and/or photoelectric effect, as per the following equation (14, 39):

$$\Delta I_{light}(t) = \left(\frac{R_o}{R(t)} - 1\right) \times I_o + \Delta I_{electric}(t),$$

where R_0, $R(t)$, I_0, and $\Delta I_{electric}(t)$ are the resistance of micropipette at room temperature, resistance of micropipette during laser illumination due to photothermal effect, holding current, and current change due to photoelectric effect, respectively. To calibrate the resistance of the micropipette as a function of temperature, the micropipette used for current measurements and the reference electrode were placed into another glass dish with preheated PBS at *ca*. 50 °C. A thermocouple was positioned close to the micropipette tip during the temperature resistance calibration measurement. The preheated PBS solution was allowed to cool down to 25 °C, and micropipette resistance was recorded as a function of temperature. The generated calibration curve follows Arrhenius relationship (14, 39, 41),

$$\ln\left(\frac{R(T)}{R_o}\right) = \frac{A}{T} + C,$$

where $R(T)$, R_0, A, T, and C are the measured resistance of the micropipette, resistance of the micropipette at room temperature, slope of the calibration curve, measured PBS temperature, and intercept of the calibration curve, respectively.

Using the above equations, the change in temperature upon laser illumination was calculated. Photothermal characterization was performed for 9 independent isolated NT-3DFG and 10 independent isolated bare i-SiNWs, with 10 measurements per wire per laser illumination condition. The average rate of change in temperature ($\Delta T/\Delta t$) was calculated as

$$\frac{\Delta T}{\Delta t} = \frac{\text{Measured Change In Temperature}}{\text{Laser Pulse Duration}}.$$

DRG Cell Isolation and Culture.

For NT-3DFG concentration viability assay and photothermal stimulation experiments. Adult male Sprague–Dawley rats (Envigo) were used. Rats weighted between 240 g and 400 g and were pair-housed with a 12:12 light:dark cycle with food and water ad libitum, at the University of Pittsburgh. Experiments were approved by the University of Pittsburgh Institutional Animal Care and Use Committee and followed the NIH guidelines for laboratory animal use. Prior to being killed, rats were anesthetized with an intraperitoneal injection of a 55 mg/kg ketamine (Henry Schein, catalog no. 056344), 5.5 mg/kg xylazine (Henry Schein, catalog no. 033197), and 1.1 mg/kg acepromazine (Henry Schein, catalog no. 003845) mixture. Rats were subsequently perfused with 1× PBS, and lumbar region DRGs were collected, enzymatically treated, and mechanically dissociated as described previously (63). The glass-bottomed dishes were treated with 50 μg/mL poly-D-lysine (PDL) (Sigma Aldrich, catalog no. P6407) and incubated for 1 h at room temperature. The dishes were rinsed three times with DI water and allowed to dry in the cell culture hood under sterile conditions for 30 min. The dishes were then treated with 20 μg/mL Laminin (Corning, catalog no. 354232) and incubated for 1 h at 37 °C. The dishes were gently rinsed with sterile 1× PBS, and the cells were seeded and incubated at 37 °C with 5% CO_2 3 h prior to flooding with Dulbecco's modified Eagle's medium (DMEM) + Glutamax (ThermoFisher, catalog no. 35050-061) supplemented with 0.1% Penicillin/Streptomycin (ThermoFisher, catalog no. 15140122), 10% fetal bovine serum (FBS) (Invitrogen, catalog no. 10082147), 10 nM/mL 2.5S neural growth factor (Sigma, catalog no. 01-125), and 10 nM/mL glial cell-derived neurotrophic factor (R&D Systems, catalog no. 212-GD-010/CF). Cells were incubated at 37 °C with 5% CO_2 for 1 d to 5 d, and 50% of the media was replaced with fresh media every 2 d.

For patch clamp experiments. DRGs were isolated from P1 to P3 Sprague–Dawley rats following decapitation and were immediately placed in ice-cold DMEM (Life Technologies, catalog no. 21063-029). DRGs were rinsed multiple times with EBSS (132 mM NaCl, 5.3 mM KCl, 10 mM Hepes, 1 mM NaH_2PO_4, 5.5 mM glucose, pH 7.4), then digested with 0.25% Trypsin (Worthington, catalog no. TRL3) in EBSS for 20 min at 37 °C under mild shaking. After digestion, the material was centrifuged for supernatant disposal and resuspended in EBSS + 10% FBS (ATCC, catalog no. 30-2020). Softened DRGs were then mechanically triturated through Pasteur pipettes of decreasing tip sizes. A final centrifugation was done, supernatant was removed, and DMEM + 5% FBS was added. Cells were seeded into sterilized PLL (Sigma-Aldrich, catalog no. P8920)-treated glass-bottomed culture dishes and allowed to sit for 30 min to facilitate DRG cell adhesion to the glass. Finally, dishes were flooded with DMEM + 5% FBS + 100 U/mL penicillin (Sigma-Aldrich, catalog no. 13750) + 100 μg/mL streptomycin (Sigma-Aldrich, catalog no. S6501) and incubated at 37 °C with 5% CO_2 until use.

Cortical Neurons Culture. Primary E18 rat cortical tissues were obtained from BrainBits LLC (SKU: SDECX). In preparation for dissociation, 2 mL of medium

from the vial was removed and placed aside for a later step. The tissues were treated with 0.25% trypsin (ethylenedinitrilo)tetraacetic acid (EDTA) solution (ThermoFisher, catalog no. 25200056) and incubated for 5 min. Post-incubation, the tissues were retreated with 0.25% trypsin EDTA solution supplemented with 0.1% DNase (ThermoFisher, catalog no. EN0521) and incubated for another 5 min. The solution was replaced by the previously removed media, and the tissue was dissociated by physical trituration five times using a sterile fire-polished glass Pasteur pipette ~1 mm in diameter, followed by another five times with a pipette smaller in diameter, that is, ~1/2 mm to 3/4 mm in diameter. The dissociated cells were then spun down at 1,100 rpm for 1 min and resuspended in 1 mL of fresh Neurobasal media (ThermoFisher, catalog no. A1413701) supplemented with 1× B27 (ThermoFisher, catalog no. A1413701), 1% Glutamax (ThermoFisher, catalog no. 35050-061), and 1% Penicillin/Streptomycin (ThermoFisher, catalog no. 15140122). The neurons were used to form cortical spheroids for photothermal stimulation (as explained below) and incubated in a 37 °C chamber with 5% CO_2 until used for experiments. Fifty percent of the cell culture media was replaced with fresh media every 3 d.

Cortical Spheroid Formation. The spheroids were formed following a previously established protocol (64). Briefly, sterile 10 g/L solution of agarose (Invitrogen, catalog no. 16500) was prepared in 0.9% (wt/vol) NaCl (Sigma, catalog no. S5886) in DI water. The agarose spherical microwells were obtained by casting the agarose into a mold (3D Petri Dish, Microtissues Inc.). The agarose microwells were equilibrated twice in Neurobasal medium for 30 min in 37 °C chamber with 5% CO_2. Cortical tissues were dissociated as mentioned above, and neurons were seeded at a density of 500,000 cells per mold in 190 μL of Neurobasal medium supplemented with 1× B27, 1% Glutamax, and 1% Penicillin/Streptomycin. The spheroids were cultured for up to 60 d, and 50% of the cell culture media was replaced with fresh media every 3 d.

NT-3DFG Suspension Preparation for NT-3DFG Concentration Viability Study. NT-3DFG were synthesized on 15 mm × 15 mm Si/SiO_2 chips with 2 μm of PECVD SiO_2 following the synthesis protocol described above. The mass of synthesized NT-3DFG was measured to be 140 ± 5 μg with a mass per unit area of 0.640 ± 0.025 μg/mm^2. The NT-3DFG samples were cleaved into 5 mm × 5 mm samples, and the effective mass of each 5 mm × 5 mm was calculated by measuring the geometric area of each chip using ImageJ (*SI Appendix*, Table S11). The cleaved NT-3DFG samples were treated with 70% wt/wt HNO_3 (CMOS Grade, J.T. Baker, catalog no. JT9606-3) for 2 h (25). The samples were rinsed three times with sterile DI water and treated overnight with 100 μg/mL lysine-phenylalanine based peptide $(KF)_4$ on a shaker (31). This was followed by washing three times with DI water. NT-3DFG were released from the Si/SiO_2 substrate by etching the SiO_2 layer in buffered HF (Alfa Aesar, catalog no. 44627) for 10 h. The released NT-3DFG were rinsed three times with sterile DI water and transferred to scintillation vials with 500 μL of sterile 1× PBS. In order to prepare the suspension, the samples were sonicated at 20 kHz and 36 W for 1 min using a probe sonicator (FB120, Fisher Scientific).

NT-3DFG Concentration Viability Assay. NT-3DFG suspensions was sterilized via UV treatment for 2 h prior to concentration preparation. NT-3DFG suspension concentrations were prepared in sterile 1× PBS as described in *SI Appendix*, Table S12. DRG neurons were cultured in glass-bottomed dishes, following the protocol described above, with DRG neuron seeding density of 1,500 cells/cm^2. Fifty microliters of each concentration was added to the cell culture dish 24 h after initial seeding (n = 4 per concentration condition). Post dosing, the DRG cell cultures were incubated for 24 h at 37 °C with 5% CO_2.

Live/Dead assay kit (ThermoFisher, catalog no. L3224) containing Calcein acetoxymethyl (Calcein AM) and Ethidium homodimer dyes was used for staining live and dead cells, respectively. Hoechst 33342 (ThermoFisher, catalog no. 62249) was used to mark the nuclei. Hoechst 33342, Calcein AM, and Ethidium homodimer dyes were added to the culture dish with a final concentration of 1 μg/mL, 2 μM, and 4 μM, respectively. The culture dishes were incubated with the dyes for 15 min at 37 °C with 5% CO_2. The samples were gently rinsed with Tyrode's buffer (Sigma, catalog no. T2145). Live-cell imaging was performed using upright confocal microscope (Nikon A1R) and a 20×/0.50 NA water immersion objective. Viability quantification was performed using four independent samples (for all concentration conditions), and five images per sample.

Viability was calculated as

$$\text{Viability}\ (\%) = \frac{\text{Total number of cells} - \text{Number Of Dead cells}}{\text{Total Number Of cells}} \times 100.$$

The density of NT-3DFG as a function of NT-3DFG concentrations was measured using differential interference contrast (DIC) images of DRG study assay and Matlab (n = 4 for each concentration, 10 independent DIC images per sample). The density of cells interfaced with NT-3DFG was measured using ImageJ (n = 4 for each concentration, five independent DIC images per samples).

DRG and NT-3DFG Interface. DRG neurons were cultured in glass-bottomed dishes following the protocol described above. One hundred μL of NT-3DFG suspension was added to the cell cultures 24 h after initial cell seeding, and the cell cultures were incubated for another 24 h at 37 °C with 5% CO_2. CellMask orange plasma membrane stain (ThermoFisher, catalog no. C10045) was used to stain the cell membrane. The cell cultures were incubated with a final concentration of 5 μg/mL of the dye for 15 min at 37 °C with 5% CO_2. The samples were gently rinsed with Tyrode's buffer. Live-cell imaging was performed using upright confocal microscope and a 20×/0.50 NA water immersion objective. The 3D reconstruction and orthogonal sections were generated using maximum intensity projection protocol in Imaris viewer (Oxford Instruments).

For SEM imaging for DRG neurons interfaced with NT-3DFG, the samples were washed three times with 1× PBS. The cell cultures were fixed using 4% paraformaldehyde (Electron Microscopy Sciences, catalog no. 15710) in 1× PBS for 20 min at room temperature. The cell cultures were then gently rinsed three times with 1× PBS for 5 min each on a shaker at room temperature. The 1× PBS was replaced with DI water. DI water was then serially replaced (25%, 50%, 75%, 90%, and 100%) with 200-proof ethanol (Pharmco-Aaper, catalog no. 111000200) with 5-min incubation at room temperature under each ethanol concentration. Critical point drying (CPD) of the samples were performed using a CPD system (Autosamdri-815, Tousimis).

NT-3DFG Sample Preparation for Photothermal Stimulation. Si/SiO_2 chips with as-grown NT-3DFG were cleaved in 1 cm × 1 cm samples, and treated with 70% wt/wt HNO_3 (CMOS Grade, J.T. Baker, catalog no. JT9606-3) for 2 h, followed by washing three times with DI water, and transferred to scintillation vials. The samples were sterilized for 2 h in 70% ethanol and air-dried in the cell culture hood for 15 min, followed by 2-h UV treatment. The samples were rinsed three times with sterile DI water and treated with 100 μg/mL lysine-phenylalanine based peptide $(KF)_4$ overnight on a shaker. The peptide solution was replaced with 500 μL of sterile 1× PBS and sonicated for 5 s to 10 s.

Photothermal Stimulation—Patch Clamp Measurements. The NT-3DFG suspension was added to the DRG culture dish and incubated for 2 h to 16 h at 37 °C with 5% CO_2. Following the incubation of peptide modified NT-3DFGs with DRG neurons, the cell culture dish was rinsed three times with recording solution (NaCl 132 mM, KCl 4 mM, $MgCl_2$ 1.2 mM, $CaCl_2$ 1.8 mM, Hepes 10 mM, glucose 5.5 mM; pH 7.4) and mounted on a microscope and visualized through 40×/0.65NA water immersion objective lens (*SI Appendix*, Fig. S14*B*). The 405-nm diode laser (HangZhou NaKu Technology) was mounted and aligned to the central axis of the microscope objective. The 405-nm laser line was TTL-modulated. Laser power was adjusted by density filters (Thorlabs). Patch pipettes were pulled on a Sutter Instruments P-2000 CO_2 laser micropipette puller (Novata) to produce 2- to 5-MΩ resistances when filled with internal pipette solution (NaCl 10 mM, KF 130 mM, $MgCl_2$ 4.5 mM, Hepes 10 mM, EGTA 9 mM, ATP 2 mM, pH 7.4). The analog waveform from a high-speed universal serial bus (USB) data acquisition device (Measurement Computing Corp., USB-1604) drove the amplifier (Axon Instruments, Axopatch 200B) to clamp the cell membrane current or voltage. Membrane potential recordings were made in current clamp mode using patch clamp amplifier and current injection with 1-ms pulse width, and *ca*. 100-nA amplitude was delivered to the neuron to assess its excitability, and, 300 ms later, laser pulses with varying pulse durations and power were applied. Laser pulses using 405-nm laser with 10-μm spot size were delivered through a 40× water immersion objective lens. Spike responses elicited by either individual pulses or pulse trains were low-pass filtered at 5 kHz by an eight-pole Bessel filter (Krohn-Hite Corp., Model 3382), digitized at 16-bit resolution and sampled at 20 kHz using patch clamp amplifier. Data acquisition and analysis was done using a custom-built software. Current recordings were made in a voltage clamp mode, and the voltage was held at −110 mV to −150 mV. Current clamp and voltage clamp measurements were performed across 12 and 3 DRG neurons, respectively.

Photothermal Stimulation—Calcium Imaging. For DRG cultures, the NT-3DFGs were drop-casted on the cells. For cortical spheroids, the spheroids were plated on PDL-coated glass-bottomed dishes and incubated overnight to promote adhesion of the tissues to the dish, followed by drop casting of the $(KF)_4$ peptide-modified NT-3DFGs. The cells/tissues were incubated with a calcium indicator dye, Cal-520 (AAT Bioquest, catalog no. 21130), for 90 min at 37 °C with 5% CO_2 followed by 30 min incubation at room temperature. The sample was washed gently three times with 1× PBS. Tyrode's buffer solution (Sigma, catalog no. T2145) was constantly perfused with carbogen gas containing 5% CO_2 and 95% O_2 (Airgas) for 20 min. The PBS in the culture dish was replaced with carbogenated Tyrode's buffer solution and loaded on the custom-built one-photon microscope setup (*SI Appendix*, Fig. S14*A*). The cell chamber was constantly perfused with fresh carbogenated Tyrode's buffer at 22 °C. The calcium imaging was performed using a 473-nm laser (UltraLasers, product no. CST-L-473-50-OEM) and green fluorescence protein (GFP) filter (Thorlabs, catalog no. MF525-39) at five frames per second, and the raw images were obtained using a Point Gray camera (FLIR, catalog no. BFS-U3-51S5C-C), operated using SpinView software. The laser pulses using 635-nm laser and 20-μm spot size were applied on the cell–wire interface through a 40×/0.80 NA water immersion objective (Nikon) using TTL pulses. The videos were generated and processed using ImageJ. For analysis, fluorescence intensities (F) for each frame were computed using ImageJ, and $(F - F_o)/F_o$ vs. time was plotted using Igor Pro software (WaveMetrics), where F_o is the minimum fluorescence used for normalization. Baseline subtraction was performed using MATLAB (MathWorks) to address the slope in the baseline due to bleaching of the dye over time. Photothermal stimulation was performed on 15 DRG neurons across five cultures, and 8 cortical tissues across three cultures.

Effect of Laser Pulse on Cell Viability. DRG neurons were seeded on glass-bottomed dishes. NT-3DFG suspension was added to the culture dish and incubated at 37 °C for 2 h. The cells were then incubated with 2 μM live cell indicator, Calcein AM dye, for 15 min at 37 °C with 5% CO_2. Post incubation, the sample was gently rinsed with carbogenated Tyrode's buffer and loaded on the microscope setup. Then 1-ms laser pulses of varying powers (2, 4, 6, 8, 10, and 22 mW) were applied on the cell–wire interface for 10 s each at 1, 5, and 10 Hz. Bright-field and fluorescent images (obtained using blue laser and GFP filter) were obtained before and after laser pulses. As a control, 1-ms laser pulses of 25-mW power at 500 Hz were applied on the cell–wire interface for 5 s, to induce cell death, indicated by the loss in fluorescence due to leakage of the Calcein AM dye. Quantification was performed on 10 DRG neurons,

$$\Delta F/F_0(\%) = \frac{F_f - F_0}{F_0} \times 100,$$

where F_0 and F_f are fluorescence values of the cell (evaluated using Matlab) before and after laser pulses, respectively.

Data Availability. All data related to the presented figures are available through Carnegie Mellon University research repository (Kilthub) at doi.org/10.1184/R1/c.4943241.v1.

ACKNOWLEDGMENTS. T.C.-K. acknowledges funding support from the NSF under Award CBET1552833, the Office of Naval Research under Award N000141712368, and the Defense Advanced Research Projects Agency under Award AWD00001593 (416052-5). B.I.P. acknowledges funding support from Pew Latin American Fellowship. S.K., C.G.E.M., and J.F.C. acknowledge support from the NSF through Grant DMR-1555001. We thank Prof. R. Davis, Dr. R. Shrestha, and Prof. S. Shen for assistance with UV-Vis measurements. We also acknowledge support from the Department of Materials Science and Engineering Materials Characterization Facility supported by Grant MCF-677785.

1. A. L. Hodgkin, A. F. Huxley, A quantitative description of membrane current and its application to conduction and excitation in nerve. *J. Physiol.* **117**, 500–544 (1952).
2. G. Hong, C. M. Lieber, Novel electrode technologies for neural recordings. *Nat. Rev. Neurosci.* **20**, 330–345 (2019).
3. E. S. Boyden, F. Zhang, E. Bamberg, G. Nagel, K. Deisseroth, Millisecond-timescale, genetically targeted optical control of neural activity. *Nat. Neurosci.* **8**, 1263–1268 (2005).
4. A. M. Packer, B. Roska, M. Häusser, Targeting neurons and photons for optogenetics. *Nat. Neurosci.* **16**, 805–815 (2013).
5. R. Chen, G. Romero, M. G. Christiansen, A. Mohr, P. Anikeeva, Wireless magnetothermal deep brain stimulation. *Science* **347**, 1477–1480 (2015).
6. G. Duret *et al*., Magnetic entropy as a proposed gating mechanism for magnetogenetic ion channels. *Biophys. J.* **116**, 454–468 (2019).
7. M. Plaksin, E. Shapira, E. Kimmel, S. Shoham, Thermal transients excite neurons through universal intramembrane mechanoelectrical effects. *Phys. Rev. X* **8**, 11043 (2018).
8. J. Wells *et al*., Optical stimulation of neural tissue in vivo. *Opt. Lett.* **30**, 504–506 (2005).
9. W. Zhou *et al*., Long term stability of nanowire nanoelectronics in physiological environments. *Nano Lett.* **14**, 1614–1619 (2014).
10. M. W. Jenkins *et al*., Optical pacing of the embryonic heart. *Nat. Photonics* **4**, 623–626 (2010).
11. J. L. Carvalho-de-Souza *et al*., Photosensitivity of neurons enabled by cell-targeted gold nanoparticles. *Neuron* **86**, 207–217 (2015).
12. Y. Fang *et al*., Texturing silicon nanowires for highly localized optical modulation of cellular dynamics. *Nano Lett.* **18**, 4487–4492 (2018).
13. J. Yong *et al*., Gold-nanorod-assisted near-infrared stimulation of primary auditory neurons. *Adv. Healthc. Mater.* **3**, 1862–1868 (2014).
14. Y. Jiang *et al*., Rational design of silicon structures for optically controlled multiscale biointerfaces. *Nat. Biomed. Eng.* **2**, 508–521 (2018).
15. C. Chiappini, X. Liu, J. R. Fakhoury, M. Ferrari, Biodegradable porous silicon barcode nanowires with defined geometry. *Adv. Funct. Mater.* **20**, 2231–2239 (2010).
16. E. Tolstik *et al*., Studies of silicon nanoparticles uptake and biodegradation in cancer cells by Raman spectroscopy. *Nanomedicine (Lond.)* **12**, 1931–1940 (2016).
17. T. J. Heikkilä *et al*., Human embryonic stem cell-derived neuronal cells form spontaneously active neuronal networks in vitro. *Exp. Neurol.* **218**, 109–116 (2009).
18. S. M. Potter, T. B. DeMarse, A new approach to neural cell culture for long-term studies. *J. Neurosci. Methods* **110**, 17–24 (2001).
19. G. Quadrato, J. Brown, P. Arlotta, The promises and challenges of human brain organoids as models of neuropsychiatric disease. *Nat. Med.* **22**, 1220–1228 (2016).
20. D. Pamies *et al*., A human brain microphysiological system derived from induced pluripotent stem cells to study neurological diseases and toxicity. *ALTEX* **34**, 362–376 (2017).
21. M. C. LaPlaca, V. N. Vernekar, J. T. Shoemaker, D. K. Cullen, "Three-dimensional neuronal cultures" in *Methods in Bioengineering: 3D Tissue Engineering*, F. Berthiaume, J. Morgan, Eds. (Artech House, 2010), pp. 187–204.
22. J. Lee, M. J. Cuddihy, N. A. Kotov, Three-dimensional cell culture matrices: State of the art. *Tissue Eng. Part B Rev.* **14**, 61–86 (2008).
23. A. Kalmykov *et al*., Organ-on-e-chip: Three-dimensional self-rolled biosensor array for electrical interrogations of human electrogenic spheroids. *Science Adv.* **5**, eaax0729 (2019).
24. G. Rossi, A. Manfrin, M. P. Lutolf, Progress and potential in organoid research. *Nat. Rev. Genet.* **19**, 671–687 (2018).
25. R. Garg *et al*., Nanowire-mesh-templated growth of out-of-plane three-dimensional fuzzy graphene. *ACS Nano* **11**, 6301–6311 (2017).
26. R. Garg *et al*., Electron transport in multi-dimensional fuzzy graphene nanostructures. *Nano Lett.* **19**, 5335–5339 (2019).
27. J. C. Meyer *et al*., The structure of suspended graphene sheets. *Nature* **446**, 60–63 (2007).
28. V. Bayot *et al*., Two-dimensional weak localization in partially graphitic carbons. *Phys. Rev. B Condens. Matter* **41**, 11770–11779 (1990).
29. D. San Roman *et al*., Engineering three-dimensional (3D) out-of-plane graphene edge sites for highly selective two-electron oxygen reduction electrocatalysis. *ACS Catal.* **10**, 1993–2008 (2020).
30. M. P. Araújo, O. Soares, A. Fernandes, M. Pereira, C. Freire, Tuning the surface chemistry of graphene flakes: New strategies for selective oxidation. *RSC Adv.* **7**, 14290–14301 (2017).
31. G.-M. Mustata *et al*., Graphene symmetry amplified by designed peptide self-assembly. *Biophys. J.* **110**, 2507–2516 (2016).
32. T. Stelzner *et al*., Silicon nanowire-based solar cells. *Nanotechnology* **19**, 295203 (2008).
33. L. Tsakalakos *et al*., Strong broadband optical absorption in silicon nanowire films. *J. Nanophotonics* **1**, 13552 (2007).
34. J.-S. Park *et al*., Enhancement of light absorption in silicon nanowire photovoltaic devices with dielectric and metallic grating structures. *Nano Lett.* **17**, 7731–7736 (2017).
35. H. Lin *et al*., A 90-nm-thick graphene metamaterial for strong and extremely broadband absorption of unpolarized light. *Nat. Photonics* **13**, 270–276 (2019).
36. P. Campbell, M. A. Green, Light trapping properties of pyramidally textured surfaces. *J. Appl. Phys.* **62**, 243–249 (1987).
37. X. Li, Z. Lv, H. Zhu, Carbon/silicon heterojunction solar cells: State of the art and prospects. *Adv. Mater.* **27**, 6549–6574 (2015).
38. A. N. Yaroslavsky *et al*., Optical properties of selected native and coagulated human brain tissues in vitro in the visible and near infrared spectral range. *Phys. Med. Biol.* **47**, 2059–2073 (2002).
39. Y. Jiang *et al*., Nongenetic optical neuromodulation with silicon-based materials. *Nat. Protoc.* **14**, 1339–1376 (2019).
40. J. L. Carvalho-de-Souza, B. I. Pinto, D. R. Pepperberg, F. Bezanilla, Optocapacitive generation of action potentials by microsecond laser pulses of nanojoule energy. *Biophys. J.* **114**, 283–288 (2018).
41. Y. Jiang *et al*., Heterogeneous silicon mesostructures for lipid-supported bioelectric interfaces. *Nat. Mater.* **15**, 1023–1030 (2016).
42. R. Parameswaran *et al*., Photoelectrochemical modulation of neuronal activity with free-standing coaxial silicon nanowires. *Nat. Nanotechnol.* **13**, 260–266 (2018).
43. Z. Li *et al*., Cellular level biocompatibility and biosafety of ZnO nanowires. *J. Phys. Chem. C* **112**, 20114–20117 (2008).

44. S. Mullick Chowdhury *et al*., Cell specific cytotoxicity and uptake of graphene nanoribbons. *Biomaterials* **34**, 283–293 (2013).
45. Y. Talukdar, J. Rashkow, G. Lalwani, S. Kanakia, B. Sitharaman, The effects of graphene nanostructures on mesenchymal stem cells. *Biomaterials* **35**, 4863–4877 (2014).
46. M. G. Shapiro, K. Homma, S. Villarreal, C.-P. Richter, F. Bezanilla, Infrared light excites cells by changing their electrical capacitance. *Nat. Commun.* **3**, 736 (2012).
47. M. S. Gold, S. Dastmalchi, J. D. Levine, Co-expression of nociceptor properties in dorsal root ganglion neurons from the adult rat in vitro. *Neuroscience* **71**, 265–275 (1996).
48. N. T. Blair, B. P. Bean, Roles of tetrodotoxin (TTX)-sensitive Na+ current, TTX-resistant Na+ current, and Ca2+ current in the action potentials of nociceptive sensory neurons. *J. Neurosci.* **22**, 10277–10290 (2002).
49. E. Loeza-Alcocer, T. P. McPherson, M. S. Gold, Peripheral GABA receptors regulate colonic afferent excitability and visceral nociception. *J. Physiol.* **597**, 3425–3439 (2019).
50. R. C. Lee, J. Hannig, "Membrane biology and biophysics" in *Surgical Research*, W. W. Souba, D. W. Wilmore, Eds. (Academic, 2001), pp. 297–305.
51. J. Akerboom *et al*., Optimization of a GCaMP calcium indicator for neural activity imaging. *J. Neurosci.* **32**, 13819–13840 (2012).
52. E. Scemes, C. Giaume, Astrocyte calcium waves: What they are and what they do. *Glia* **54**, 716–725 (2006).
53. J. Lallouette, M. De Pittà, H. Berry, "Astrocyte networks and intercellular calcium propagation" in *Computational Glioscience*, M. De Pittà, H. Berry, Eds. (Springer, 2019), pp. 177–210.
54. M. J. Berridge, Neuronal calcium signaling. *Neuron* **21**, 13–26 (1998).
55. T. Hartung, Thoughts on limitations of animal models. *Parkinsonism Relat. Disord.* **14** (suppl. 2), S81–S83 (2008).
56. E. Cukierman, R. Pankov, D. R. Stevens, K. M. Yamada, Taking cell-matrix adhesions to the third dimension. *Science* **294**, 1708–1712 (2001).
57. M. Hindié *et al*., Interactions of B16F10 melanoma cells aggregated on a cellulose substrate. *J. Cell. Biochem.* **99**, 96–104 (2006).
58. H. R. Irons *et al*., Three-dimensional neural constructs: A novel platform for neurophysiological investigation. *J. Neural Eng.* **5**, 333–341 (2008).
59. J. Kawada *et al*., Generation of a motor nerve organoid with human stem cell-derived neurons. *Stem Cell Reports* **9**, 1441–1449 (2017).
60. E. J. Gualda, D. Simão, C. Pinto, P. M. Alves, C. Brito, Imaging of human differentiated 3D neural aggregates using light sheet fluorescence microscopy. *Front. Cell. Neurosci.* **8**, 221 (2014).
61. A. Lee *et al*., 3D bioprinting of collagen to rebuild components of the human heart. *Science* **365**, 482–487 (2019).
62. S. K. Rastogi *et al*., Three-dimensional fuzzy graphene ultra-microelectrodes for subcellular electrical recordings. *Nano. Res.*, 10.1007/s12274-020-2695-y (2020).
63. S. G. Lu, X. Zhang, M. S. Gold, Intracellular calcium regulation among subpopulations of rat dorsal root ganglion neurons. *J. Physiol.* **577**, 169–190 (2006).
64. A. P. Napolitano *et al*., Scaffold-free three-dimensional cell culture utilizing micromolded nonadhesive hydrogels. *Biotechniques* **43**, 494–500, 496–500 (2007).